Lifetime measurements of yrast states in ^{162}Yb and ^{166}Hf

E. A. McCutchan,[1] N. V. Zamfir,[1,2] R. F. Casten,[1] H. Ai,[1] H. Amro,[1] M. Babilon,[1,3] D. S. Brenner,[4] G. Gürdal,[1,4] A. Heinz,[1] R. O. Hughes,[1,5] D. A. Meyer,[1] C. Plettner,[1] J. Qian,[1] J. J. Ressler,[1] N. J. Thomas,[1,5] V. Werner,[1] E. Williams,[1] and R. Winkler[1]

[1]*Wright Nuclear Structure Laboratory, Yale University, New Haven, Connecticut 06520 USA*

[2]*National Institute of Physics and Nuclear Engineering, Bucharest-Magurele, Romania*

[3]*Institut für Kernphysik, Technische Universität Darmstadt, D-64289, Germany*

[4]*Clark University, Worcester, Massachusetts 01610*

[5]*University of Surrey, Guildford, Surrey GU2 7XH, United Kingdom*

(Received 23 December 2005; published 9 March 2006)

Lifetime measurements of yrast levels in ^{162}Yb and ^{166}Hf were performed using the recoil distance Doppler-shift method in coincidence mode. Excited states in ^{162}Yb and ^{166}Hf were populated via the reactions ^{116}Cd(^{50}Ti, 4n) and ^{122}Sn(^{48}Ti, 4n), respectively. The resulting $B(E2)$ values are compared with the X(5) critical point model predictions and interacting boson approximation (IBA) model calculations. The X(5) model provides a reasonable description of the yrast $B(E2)$ values in ^{166}Hf, whereas the IBA fails to reproduce the transition strengths from the higher spin levels. In ^{162}Yb, some transitions agree with the X(5) predictions while others are more consistent with the predictions of the IBA or a deformed symmetric rotor.

DOI: 10.1103/PhysRevC.73.034303 PACS number(s): 21.10.Tg, 21.60.Ev, 25.70.Hi, 27.70.+q

I. INTRODUCTION

Nuclei have been traditionally described relative to the standard benchmarks of nuclear structure: the harmonic vibrator [1], the symmetrically deformed rotor [2], and the deformed γ-soft model [3]. "Newer" benchmarks of structure for describing nuclei transitional between these structures have recently been proposed [4,5] with particular focus on the critical point of spherical to deformed transitions. The X(5) critical point model [5] describes nuclei at the critical point of the transition from spherical to axially symmetric deformed within the framework of the Bohr Hamiltonian. The nuclear potential is approximated as an infinite square well with respect to the β degree of freedom and a harmonic oscillator with respect to the γ degree of freedom. The β and γ degrees of freedom are decoupled and allow for parameter-free (except for scale) analytic predictions for excitation energies and electromagnetic transition strengths.

Empirical realizations of the X(5) critical point model were subsequently identified, with a concentration of examples observed in the $N = 90$ rare earth nuclei. Despite the approximations involved in the decoupling of the β and γ degrees of freedom [6], the model works very well. In terms of both energies and electromagnetic transition strengths, ^{150}Nd [7], ^{152}Sm [8], ^{154}Gd [9], and ^{156}Dy [10] have been shown to exhibit properties similar to the X(5) predictions. The success of the X(5) model in describing the properties of these nuclei has led to tremendous interest in phase transitional behavior. For example, since the development of X(5), numerous modifications (see, for example Refs. [11–13]) have been proposed and investigations into phase transitional behavior in this mass region (see, for example Refs. [14,15]) have been performed.

The identification of additional nuclei exhibiting an X(5)-like structure with $N \neq 90$ will test whether this concept of critical point nuclei is of wider scope or unique to the $N = 90$ isotones. Classification of a nucleus in terms of X(5) requires an extensive comparison of excitation energies and electromagnetic transition strengths. For example, ^{104}Mo was first interpreted in terms of an X(5) structure [16] based on excitation energies and branching ratios. An ensuing measurement of yrast $B(E2)$ values in ^{104}Mo [17] found a discrepancy with the X(5) model. A similar inconsistency is observed in the nuclei ^{162}Yb ($N = 92$) and ^{166}Hf ($N = 94$). As shown in Fig. 1(a), the yrast energies [18,19] of both of these nuclei are very close to the X(5) predictions. Recent experiments [20,21] on these nuclei have established that the low-spin, non-yrast states also resemble the X(5) predictions. However, an interpretation in terms of the X(5) model becomes difficult, if not fails, when considering the previously known electromagnetic transition probabilities of the yrast sequence, as shown in Figs. 1(b) and 1(c). In ^{162}Yb, two separate experiments [22,23] give lifetimes which show some discrepancies, particularly for the 6_1^+ level. In both measurements, the yrast $B(E2)$ values lie either close to or below the rotor predictions for spin 6_1^+ and higher. In ^{166}Hf, lifetimes were measured in a single experiment [24], and an X(5) structure cannot be excluded, but the error bars are far too large to allow for a useful comparison.

The purpose of this work is to report on the new measurement of yrast level lifetimes in ^{162}Yb and ^{166}Hf. Previous measurements [22–24] of yrast level lifetimes in these nuclei were determined using the recoil distance Doppler shift (RDDS) method in singles mode. The present work makes use of the RDDS method in coincidence mode, eliminating problems caused by both unobserved and observed level sidefeeding. Furthermore, application of the differential decay curve method (DDCM) in the analysis allows for the detection of systematic errors, resulting in an improved measurement of level lifetimes. Besides the measurement of the lifetimes themselves, a key aspect of this study is the significant reduction (often a factor of 3 or more) in the uncertainties. This is crucial to providing an adequate test of X(5). For example, for the $6_1^+ \rightarrow 4_1^+$ and $8_1^+ \rightarrow 6_1^+$ transitions, the X(5) and rotor

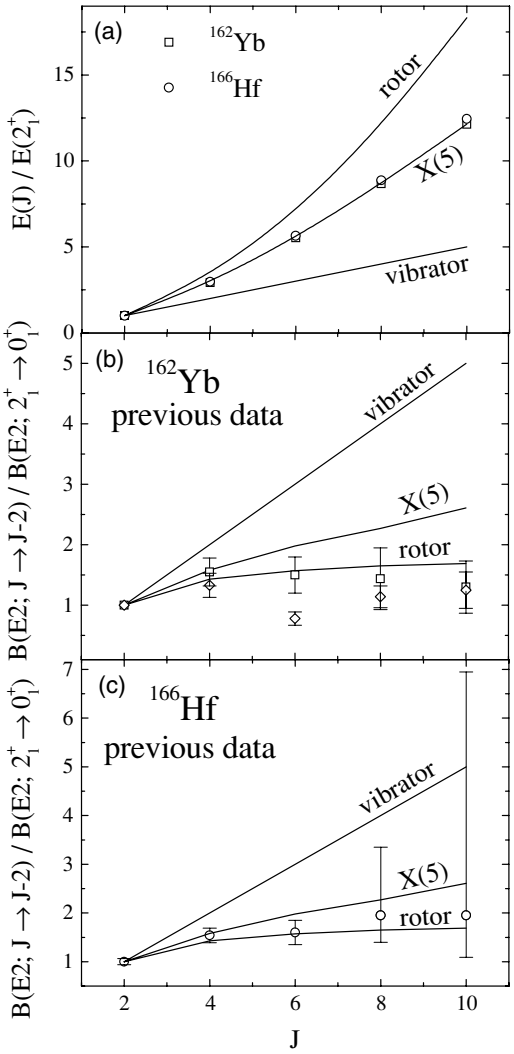

FIG. 1. (a) Yrast band energies in ^{162}Yb and ^{166}Hf normalized to the 2_1^+ energy. Data are taken from Refs. [18,19]. Previously known $B(E2)$ values in ^{162}Yb (b) and ^{166}Hf (c), normalized to the $B(E2; 2_1^+ \rightarrow 0_1^+)$ value in each nucleus. Experimental $B(E2)$ values in ^{162}Yb are derived from lifetimes in Ref. [22] (□) and Ref. [23] (◇) and in ^{166}Hf from Ref. [24]. The X(5), rotor, and vibrator predictions are included for comparison.

predictions differ by 20%–30%, which is comparable to the uncertainties in the existing measurements. These lifetime measurements will provide a more stringent test of descriptions of these nuclei.

II. EXPERIMENT AND DATA ANALYSIS

Lifetimes of excited states in ^{162}Yb and ^{166}Hf were measured using the RDDS method in coincidence mode. States in ^{162}Yb were populated via the ^{116}Cd(^{50}Ti, $4n$) reaction and states in ^{166}Hf were populated via the ^{122}Sn(^{48}Ti, $4n$) reaction. Each experiment was performed with a 200 MeV Ti beam delivered by the ESTU tandem accelerator at the Wright Nuclear Structure Laboratory at Yale University. The ^{162}Yb experiment was performed with a ∼0.3 pnA ^{50}Ti beam, while the ^{166}Hf experiment used a 1–2 pnA ^{48}Ti beam. Both experiments used a 1.0 mg/cm^2 self-supporting target foil, and recoiling nuclei were stopped in a 10 mg/cm^2 thick Au foil. The target and stopper foil were mounted in the new Yale plunger device (NYPD) [25], which is based on the design of the Cologne plunger [26].

The recoiling nuclei exited the target with a mean velocity of $v = 0.022(1)\ c$ for ^{166}Hf and $v = 0.020(1)\ c$ for ^{162}Yb. Data were collected for 15 target-to-stopper distances ranging from 5 to 500 μm for 4 to 12 h each, with the longer runs corresponding to the shorter distances in order to be sensitive to shorter lifetimes. In order to correct for thermal drifts in the foils resulting from beam heating, the plunger system uses an automatic feedback system. The capacitance between the target and stopper foils was continuously monitored and corrections for any fluctuations were made. The accuracy of the measurement of the relative target-to-stopper distances was better than 0.2 μm in the range from electrical contact to 20 μm and ∼2% of the target-to-stopper separation in the range 20–200 μm.

γ rays were detected with the SPEEDY array [27], consisting of eight Compton-suppressed HPGe clover detectors. The detectors were evenly distributed between two rings at angles of 41.5° and 138.5° with respect to the beam axis. For each target-to-stopper distance, data were sorted into four γ-γ matrices corresponding to all combinations of the two rings. Spectra for different target-to-stopper distances were normalized by setting gates on the shifted and unshifted peaks of the $4_1^+ \rightarrow 2_1^+$ and $6_1^+ \rightarrow 4_1^+$ γ-ray transitions and requiring that the sum of the shifted and unshifted components of higher lying γ-ray transitions remained constant for all distances. The sum of the total number of events in each coincidence matrix was used as a consistency check of the normalization procedure. The quality of the gated spectra for each experiment is illustrated in Fig. 2. Gates are placed on the shifted component of the $6_1^+ \rightarrow 4_1^+$ transitions in ^{162}Yb and ^{166}Hf and show the decay of the 4_1^+ state at three different target-to-stopper distances.

Level lifetimes were determined with the differential decay curve method (DDCM) [28,29] applied in coincidence mode. A gate was placed on the shifted component of a feeding γ-ray transition, and the intensities of the Doppler shifted and unshifted components of the γ-ray transition depopulating the level of interest were measured for each target-to-stopper distance. By placing a gate on feeding transitions, a particular decay path was selected and any contributions from known or unknown sidefeedings were eliminated. For a level of interest populated directly (indirectly) by transition B (C) and depopulated by transition A, the lifetime $\tau(x)$ was obtained by [28,29]

$$\tau(x) = \frac{I_{\rm su}^{CA}(x) - \alpha I_{\rm su}^{CB}(x)}{v \frac{d}{dx} I_{\rm ss}^{CA}(x)} \qquad (1)$$

where v is the recoil velocity, x is the target-to-stopper distance, and the factor α is given by

$$\alpha = \frac{I_{\rm su}^{CA}(x) + I_{\rm ss}^{CA}(x)}{I_{\rm su}^{CB}(x) + I_{\rm ss}^{CB}(x)}. \qquad (2)$$

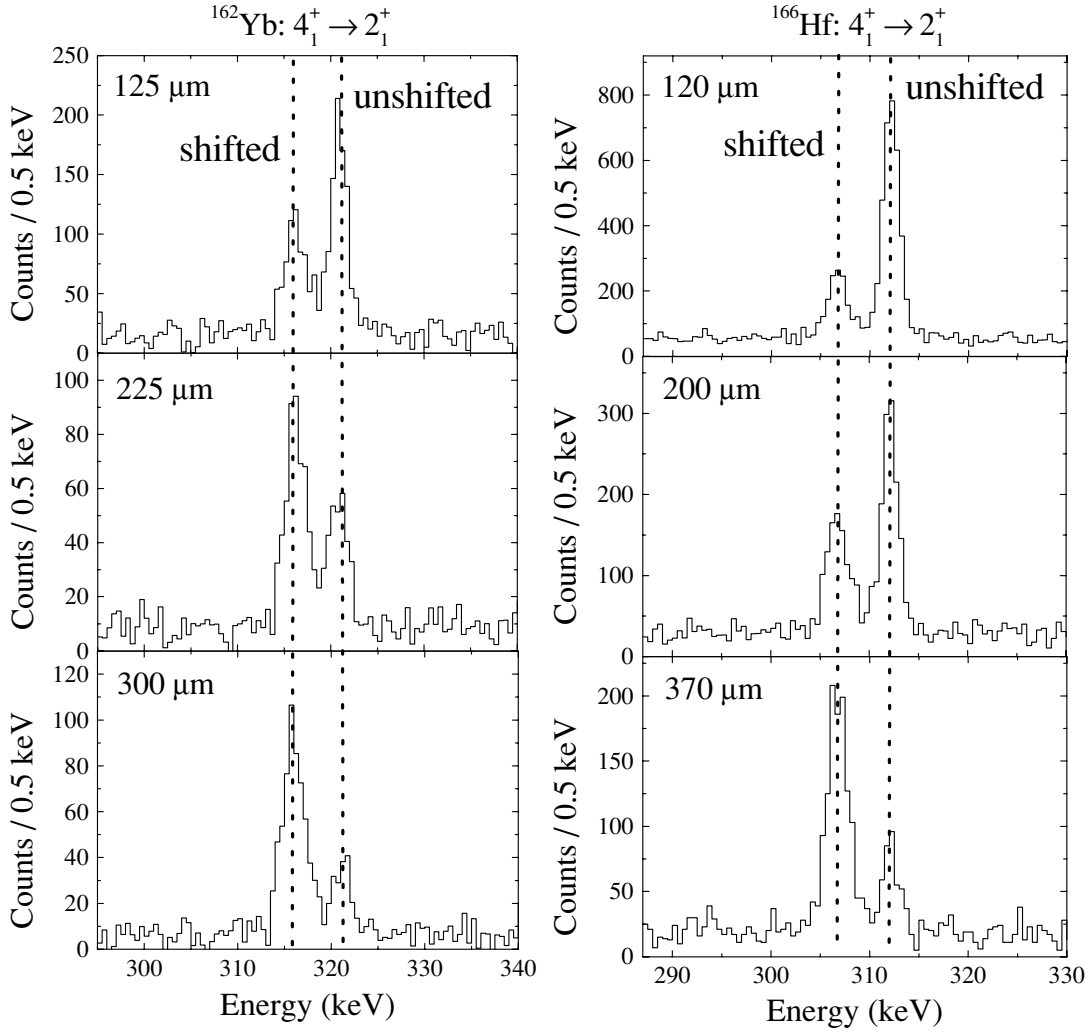

FIG. 2. Sample γ-γ coincidence spectra for ^{162}Yb and ^{166}Hf. Gates are placed on the $6_1^+ \rightarrow 4_1^+$ transition in each nucleus showing the shifted and unshifted components of the $4_1^+ \rightarrow 2_1^+$ transition at three different target-to-stopper distances. Spectra are from the detectors at backward angles (138.5°).

The intensities I_{ss}^{CA}, I_{su}^{CA} are the number of coincidences between the shifted (s) component of an indirect feeding transition C and the shifted (s) or unshifted (u) component of the depopulating transition A of the level of interest, respectively. The numerator is calculated directly for each target-to-stopper distance. The denominator is determined by fitting piecewise continuously differentiable second-order polynomials to the measured intensities of I_{ss}^{CA}. When gates are set on a directly populating γ-ray transition B, Eq. (1) reduces to

$$\tau(x) = \frac{I_{su}^{BA}(x)}{v\frac{d}{dx}I_{ss}^{BA}(x)}. \tag{3}$$

In the ideal case, the calculated values of $\tau(x)$ for each distance are the same. The ability to obtain several independent lifetime values for a given level provides a consistency check of the results and allows for the identification of systematic errors in the measurement or analysis. A detailed description of this method is given in Refs. [28,29].

III. EXPERIMENTAL RESULTS

In the present work, the lifetimes of excited states in ^{166}Hf and ^{162}Yb were obtained. When possible, independent lifetime values were obtained for each angular grouping of detectors. The following discussion concentrates on the analysis of the 4_1^+, 6_1^+, and 8_1^+ levels in ^{166}Hf and ^{162}Yb. For reference, Fig. 3 gives partial level schemes for ^{166}Hf and ^{162}Yb relevant to the discussion. Selected results from the analysis are illustrated in Figs. 4–7. Additional lifetimes for a few higher lying states in both ^{166}Hf and ^{162}Yb were also measured. The complete results of the DDCM analysis are summarized in Table I.

A. ^{166}Hf

The 4_1^+ level is populated by a 426.6 keV transition and depopulated by a 311.8 keV transition. The presence of a 418.1 keV, $11_1^- \rightarrow 9_1^-$ transition prevented placing a gate on the backward-shifted component of the populating transition.

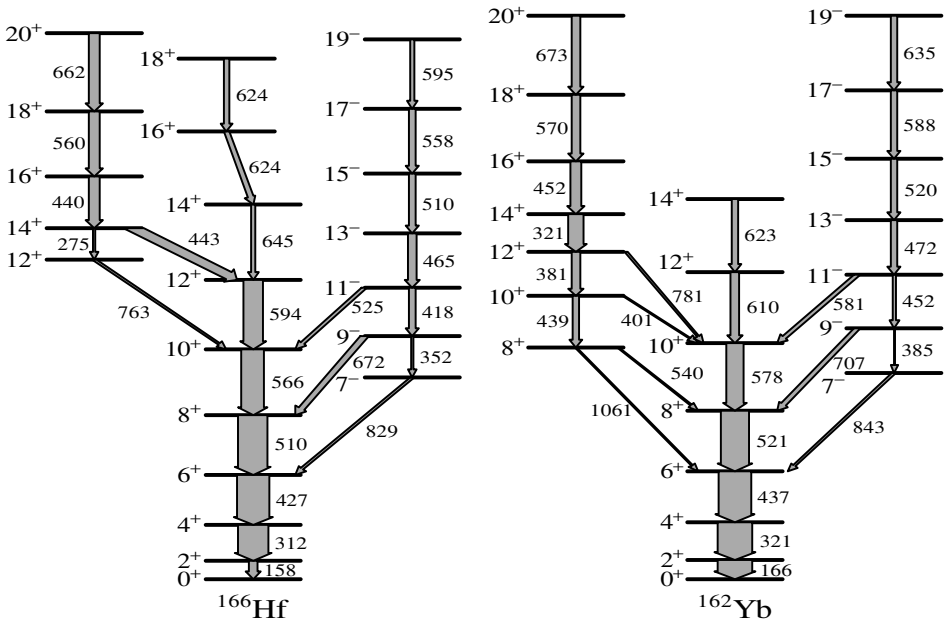

FIG. 3. Partial level scheme of ^{166}Hf and ^{162}Yb. γ-ray transition energies are labeled and the widths of the arrows are approximately proportional to the γ-ray intensities in these experiments.

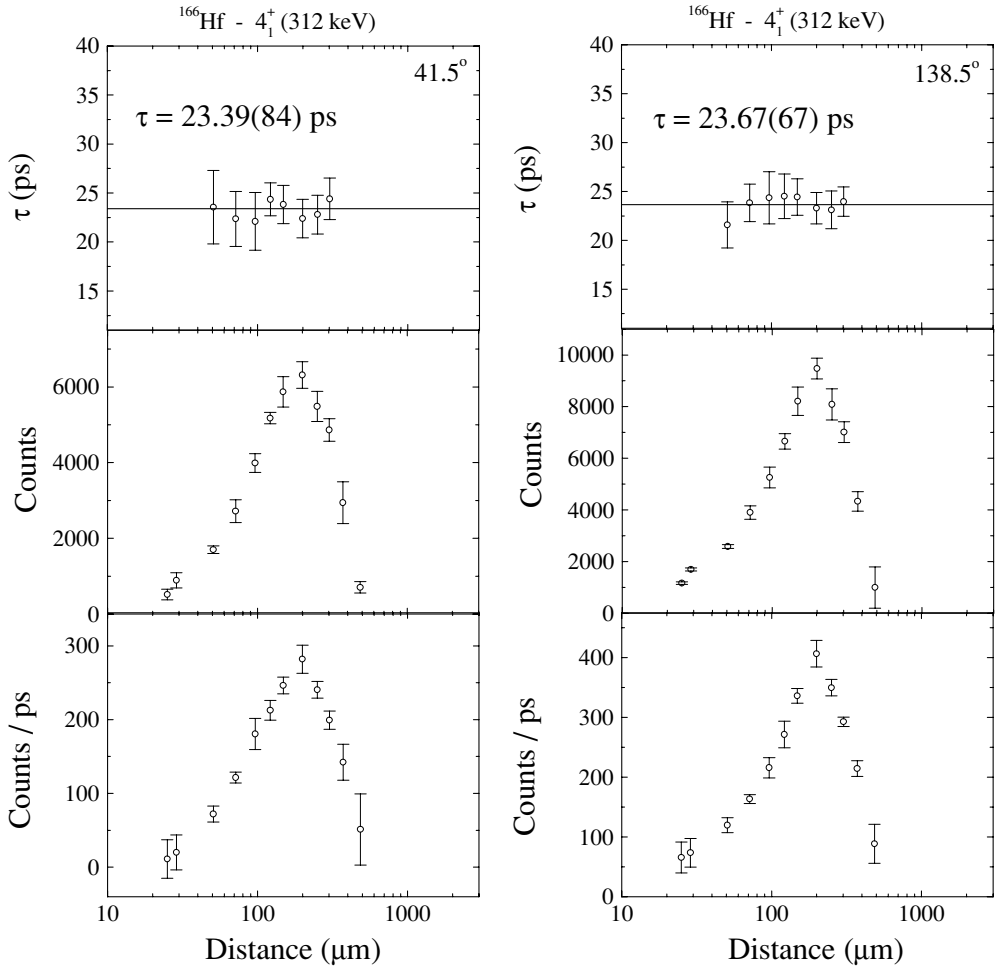

FIG. 4. DDCM analysis of the 4_1^+ state in ^{166}Hf obtained through a direct gate on the forward shifted $6_1^+ \rightarrow 4_1^+$ transition and analyzing the depopulating transition at forward (left) and backward (right) angles. Lower panels correspond to the derivative of the shifted component of the 4_1^+ decay curve. Middle panels give the unshifted component of the $4_1^+ \rightarrow 2_1^+$ transition as a function of distance. Upper panels give the resulting lifetime of the level, τ, obtained by calculating the ratio of the middle and lower panels [Eq. (3)]. Only those values of τ included in the final lifetime evaluation are included in the upper panel (see text).

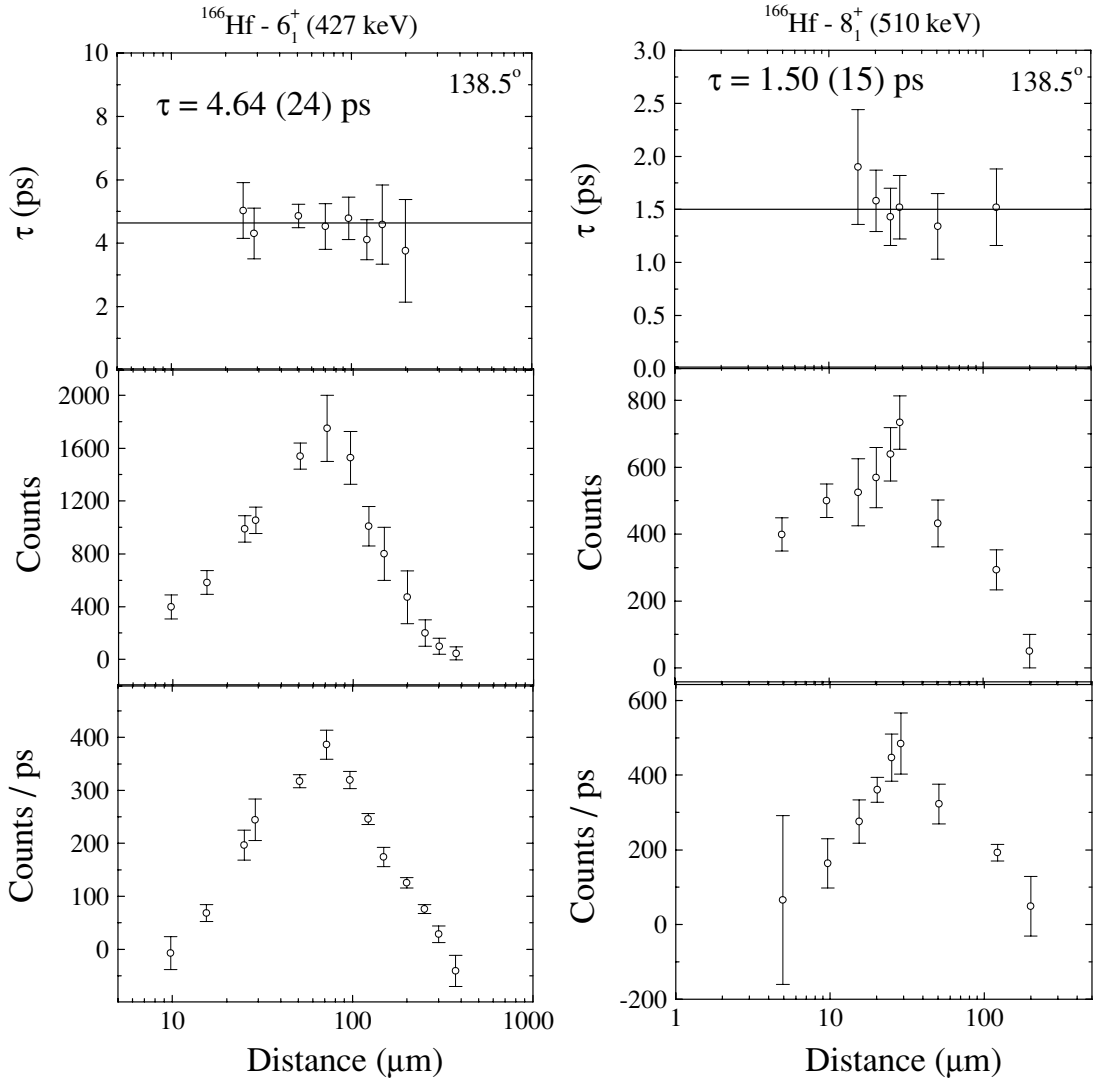

FIG. 5. Same as in Fig. 4, but for the 6_1^+ (left) and 8_1^+ (right) levels of ^{166}Hf. The lifetime of the 6_1^+ level was obtained by an indirect gate [Eq. (1)] on the $10_1^+ \rightarrow 8_1^+$ γ-ray transition, while the 8_1^+ level lifetime was obtained through a gate on a direct populating transition [Eq. (3)].

The results of the analysis from gating on the forward-shifted 427 keV, $6_1^+ \rightarrow 4_1^+$ transition and measuring the shifted and unshifted components of the 312 keV, $4_1^+ \rightarrow 2_1^+$ transition in both the forward and backward rings are shown in Fig. 4. The bottom panel gives the x derivative of the intensity of the shifted peak corresponding to the denominator of Eq. (3). The numerator of Eq. (3), the intensity of the unshifted peak, is illustrated in the middle panel. The lifetime, τ (top panel), is the ratio of the middle and bottom panels. The range of distances used for evaluating the mean τ is limited to the sensitive region of the measurement, where the numerator and denominator of Eq. (3) are not close to zero. The lifetime curves obtained for both forward and backward angles (Fig. 4), show consistent agreement. The present lifetime value of 23.5(9) ps is consistent within error with the previous measurement [24] of 24.2(14) ps.

In evaluating the lifetime of the 6_1^+ level, a direct gate on the 509.5 keV feeding transition was not possible, because the 510 keV transition is coincident with the 418 keV, $11_1^- \rightarrow 9_1^-$ transition, contaminating the shifted 427 keV peak at backward angles and the unshifted 427 keV peak at forward angles. Therefore, it was necessary to gate on other transitions in the band, noncoincident with the 418 keV transition. The analysis given in Fig. 5 (left) is a result of gating indirectly on the 565.5 keV, $10_1^+ \rightarrow 8_1^+$ transition and applying Eq. (1). The resulting lifetime of 4.6(3) ps is consistent within error with the previous measurement [24] and provides a factor of 2 reduction in the uncertainty.

The lifetime of the 8_1^+ level was obtained through a direct gate on the 565.5 keV, $10_1^+ \rightarrow 8_1^+$ transition. Statistics in the backward gated spectra were limited because of the presence of the strong 560 keV, $18_1^+ \rightarrow 16_1^+$ transition which restricted the width of the gate on the populating transition. Figure 5 (right) illustrates the τ curve obtained by gating on forward-shifted components of the feeding transition. The resulting lifetime of 1.50 (15) ps is consistent within error with the previous measurement [24] and provides nearly a factor of 5 reduction in the uncertainty.

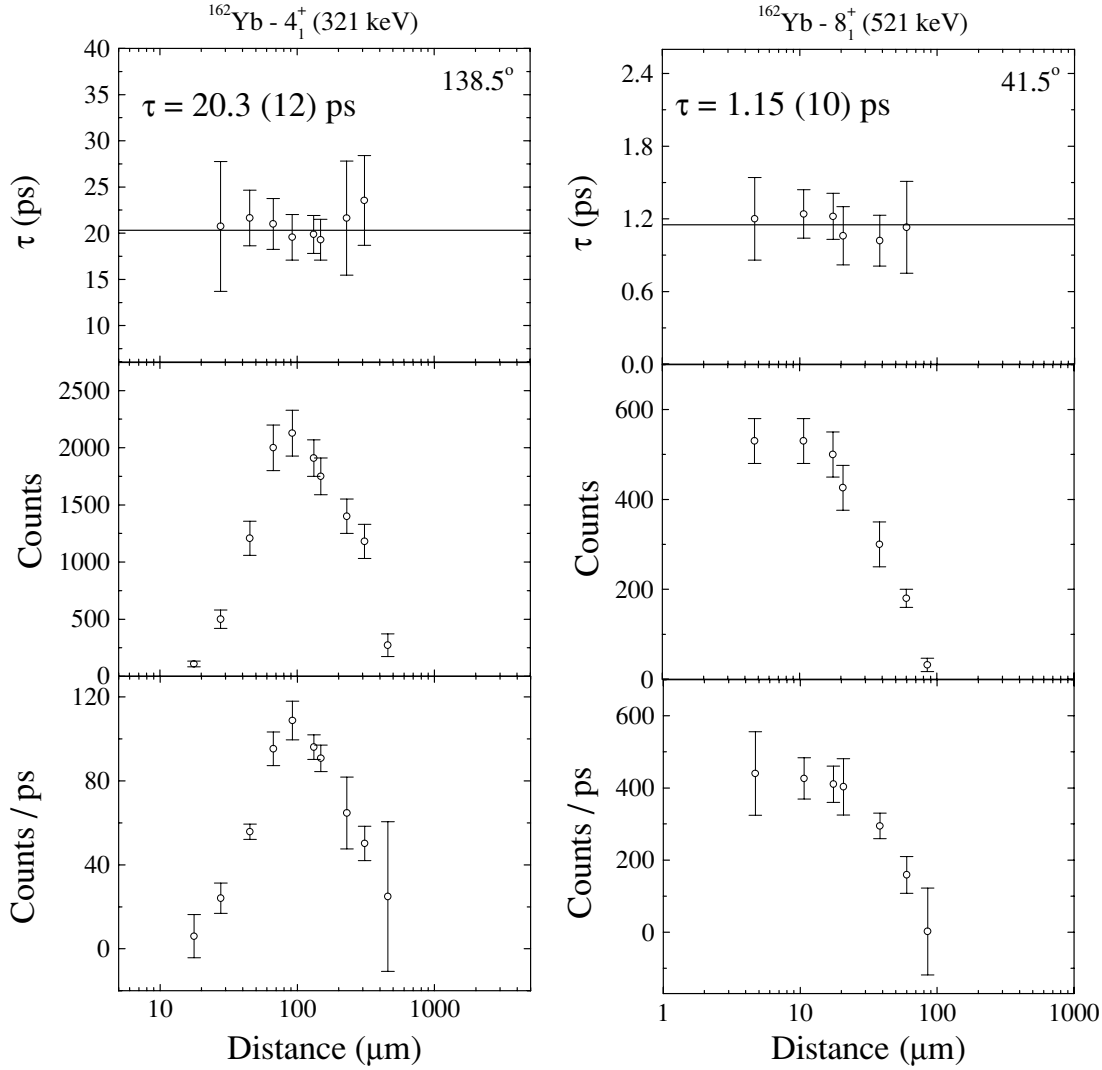

FIG. 6. Same as in Fig. 4, but for the 4_1^+ (left) and 8_1^+ (right) levels of ^{162}Yb. The lifetime of the 4_1^+ level was obtained by an indirect gate [Eq. (1)] on the $10_1^+ \rightarrow 8_1^+$ γ-ray transition, while the 8_1^+ level lifetime was obtained through a gate on a direct populating transition [Eq. (3)].

B. ^{162}Yb

The 4_1^+ state is populated by a 436.7 keV transition and depopulated by a 320.6 keV transition. Difficulties in determining this lifetime arise from the presence of two strong contaminant lines: a 439.1 keV, $10_2^+ \rightarrow 8_2^+$ transition and a 320.6 keV, $14_1^+ \rightarrow 12_2^+$ transition. The former makes a direct gate on the feeding transition difficult, while the latter contaminates the shifted and unshifted components of the depopulating transition. It was found that a clean gate could be obtained by placing an indirect gate on the 578 keV, $10_1^+ \rightarrow 8_1^+$ transition. The result of the τ analysis is given in Fig. 6 (left). The lifetime obtained ($\tau = 20.5(9)$ ps) is consistent within error with the previous two measurements [22,23] and gives a factor of 3 reduction in the uncertainty.

The 6_1^+ state is populated by a 521.3 keV transition and depopulated by a 436.7 keV transition. A direct gate on the 521 keV transition yields a lifetime of 5.1 (4) ps, as shown in Fig. 7 (left). Gates were only placed on forward-shifted components since the backward-shifted ones were contaminated by the 511 keV annihilation line. The direct gate on the $8_1^+ \rightarrow 6_1^+$ transition is weakly coincident with the 439.1 keV, $10_2^+ \rightarrow 8_2^+$ transition. To confirm that this does not affect the resulting lifetime, an indirect gate on the 578.4 keV, $10_1^+ \rightarrow 8_1^+$ transition was also performed. The result of the τ analysis is given in Fig. 7 (right). Both the direct gate and the indirect gate yield a consistent lifetime of 5.0(3) ps. The present result favors the lower of the previous two measurements [23] and gives a factor of 3 reduction in the uncertainty [Table I].

The lifetime of the 8_1^+ level was obtained through a direct gate on the 578 keV, $10_1^+ \rightarrow 8_1^+$ transition. The presence of a strong 570 keV, $18_1^+ \rightarrow 16_1^+$ transition prevented placing a gate on the backward-shifted component of the direct feeding transition. Figure 6 (right) gives the τ curve obtained by gating on the forward-shifted components of the feeding transition. The resulting lifetime of 1.2(3) ps is less than the previous measurements, yet it still agrees within error with the result of Ref. [23].

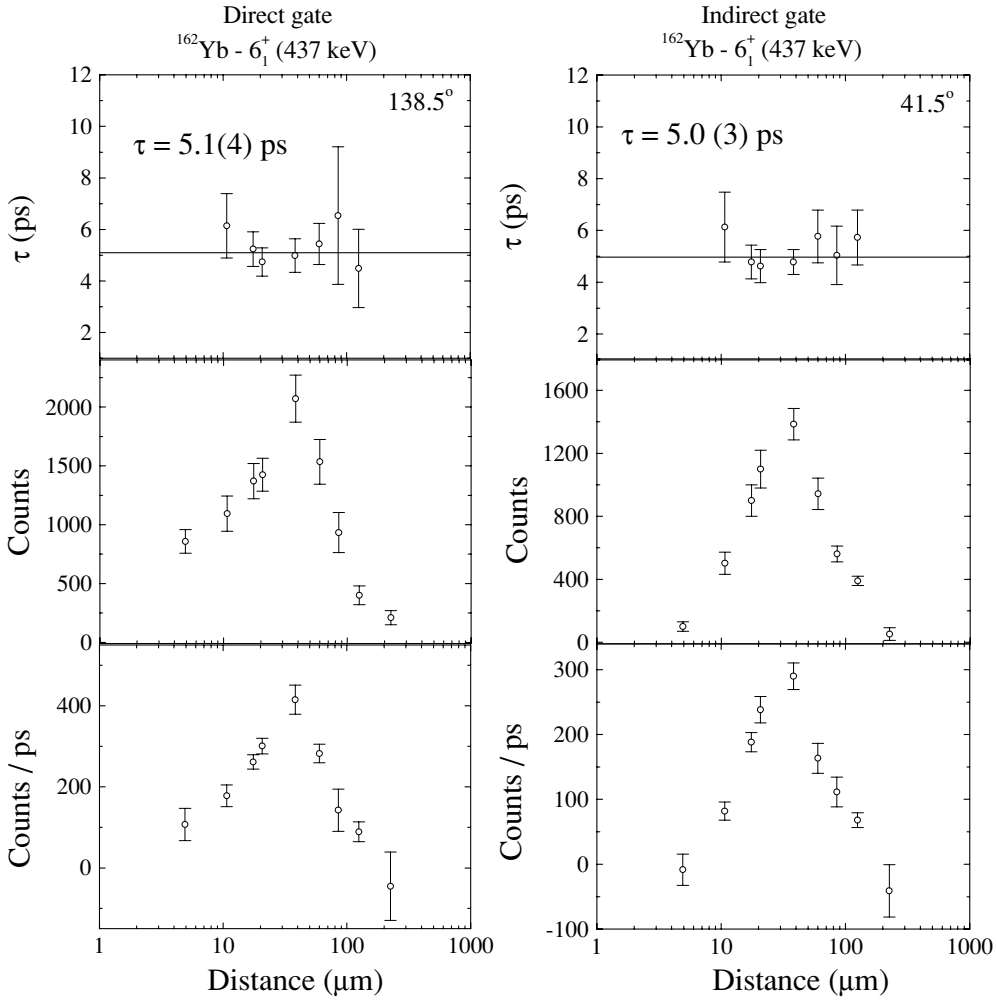

FIG. 7. Same as in Fig. 4, but for the 6_1^+ level of ^{162}Yb. The lifetime was obtained through a direct gate [Eq. (3)] on the $8_1^+ \rightarrow 6_1^+$ transition (left) and an indirect gate [Eq. (1)] on the $10_1^+ \rightarrow 8_1^+$ transition (right).

TABLE I. Analyzed transitions, derived lifetimes τ, literature lifetimes, experimental $B(E2)$ values (corresponding to τ values obtained in this work) and X(5) and IBA theoretical predictions.

Nucleus	Transition	E_γ (keV)	$\tau_{present}$ (ps)	τ_{lit} (ps)	$B(E2)_{exp}$ (W.u.)	$B(E2)_{X(5)}$ (W.u.)	$B(E2)_{IBA}$ (W.u.)
^{166}Hf	$2_1^+ \rightarrow 0_1^+$	159		717(33)1[a]	128(8)	128	128
	$4_1^+ \rightarrow 2_1^+$	312	23.5(9)	24.2(14)1[a]	203(8)	202	188
	$6_1^+ \rightarrow 4_1^+$	427	4.6(3)	5.0(7)1[a]	225(20)	253	209
	$8_1^+ \rightarrow 6_1^+$	510	1.50(15)	1.7(7)1[a]	293(30)	291	216
	$14_1^+ \rightarrow 12_1^+$	443	10.0(10)		70(10)	365	185
	$9_1^- \rightarrow 7_1^-$	352	2.5(5)		237(50)		
^{162}Yb	$2_1^+ \rightarrow 0_1^+$	167		583(17)2[b]	138(5)	138	138
	$4_1^+ \rightarrow 2_1^+$	321	20.5(9)	20.3(30)3[c], 23.4(36)4[d]	219(11)	218	201
	$6_1^+ \rightarrow 4_1^+$	437	5.0(3)	4.6(9)3[c], 8.8(12)4[d]	194(10)	273	224
	$8_1^+ \rightarrow 6_1^+$	521	1.2(3)	2.0(7)3[c], 2.5(4)4[d]	305(75)	313	231
	$14_1^+ \rightarrow 12_2^+$	321	25(10)	53(9)4[d]	178(75)		
	$16_1^+ \rightarrow 14_1^+$	452	4.7(3)	4.5(7)4[d]	171(27)	412	170

[a]Reference [19], which is based on Ref. [24].
[b]Reference [18].
[c]Reference [22].
[d]Reference [23].

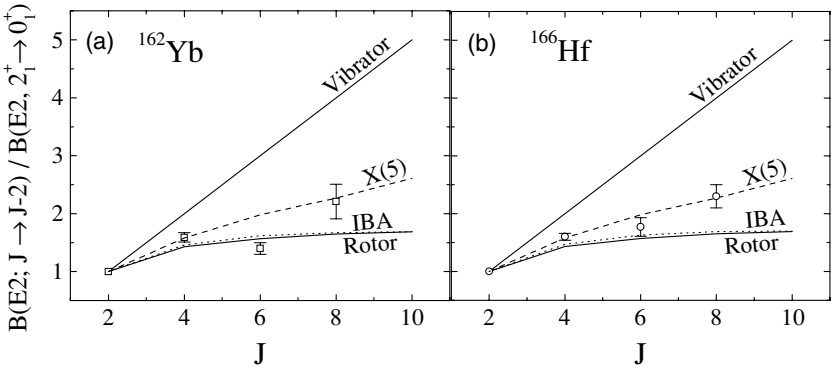

FIG. 8. $B(E2)$ values derived in the present work for ^{162}Yb (a) and ^{166}Hf (b), normalized to the experimental $B(E2;\ 2_1^+ \rightarrow 0_1^+)$ value in each nucleus. The X(5), IBA, rotor, and vibrator predictions are included for comparison.

IV. DISCUSSION

The nuclei ^{162}Yb and ^{166}Hf lie close to a region where X(5)-like structures have been well established. Investigating the extent of X(5) behavior in rare-earth nuclei should lead to a better understanding of critical point nuclei. In this section, the new lifetime measurements obtained in this work are used to compare the revised decay properties of yrast states in ^{162}Yb and ^{166}Hf to the X(5) predictions [5] as well as the predictions of the interacting boson approximation (IBA) model [30].

The nuclei ^{162}Yb and ^{166}Hf exhibit energy spectra very similar to the predictions of the X(5) critical point model. An extensive comparison of the energy spectrum of ^{162}Yb and ^{166}Hf with X(5) was shown previously [20,21]. To summarize, the key energy predictions of X(5) involve the ratios $R_{4/2} \equiv E(4_1^+)/E(2_1^+) = 2.90$ and $R_{0/2} \equiv E(0_2^+)/E(2_1^+) = 5.67$. Similar ratios are observed experimentally in ^{162}Yb and ^{166}Hf with $R_{4/2} = 2.93,\ 2.97$ and $R_{0/2} = 6.0,\ 6.7$, respectively. As mentioned previously, however, electromagnetic transition probabilities provide a more rigorous test of the structure of a nucleus and its interpretation in terms of X(5) character.

The new lifetime measurements of yrast levels in ^{162}Yb and ^{166}Hf, particularly the resulting large reduction in uncertainties, provides much improved information on yrast $B(E2)$ strengths in these nuclei. From the newly measured lifetimes, the resulting $B(E2)$ values for the transitions were determined. Conversion coefficients used in the calculation of $B(E2)$ strengths were taken from Refs. [18,19]. All results are summarized in Table. I. The yrast electromagnetic transition probabilities obtained in this work are also shown in Fig. 8, along with the predictions of X(5), the vibrator, and the symmetric rotor. In Fig. 8, all values are normalized to the experimental $B(E2;\ 2_1^+ \rightarrow 0_1^+)$ value. Note that with this normalization, the X(5) predictions involve no free parameters.

In ^{162}Yb, the experimental $B(E2;\ 4_1^+ \rightarrow 2_1^+)$ value agrees very well with the X(5) prediction. However, the experimental $B(E2;\ 6_1^+ \rightarrow 4_1^+)$ value shows little agreement with the X(5) model. It lies significantly below the X(5) predictions and even below the rotor predictions. It is interesting to note that similar behavior in the $6_1^+ \rightarrow 4_1^+$ transition is observed in the X(5) candidate nucleus, ^{156}Dy [31]. Continuing higher in spin, the experimental $B(E2;\ 8_1^+ \rightarrow 6_1^+)$ value is again in good agreement with the X(5) prediction.

In ^{166}Hf, the experimental $B(E2;\ 4_1^+ \rightarrow 2_1^+)$ value shows good agreement with the X(5) prediction. The experimental $B(E2;\ 6_1^+ \rightarrow 4_1^+)$ value lies intermediate between the X(5) and rotor values, just outside of the X(5) prediction when considering the error. A similar dip in the $B(E2;\ 6_1^+ \rightarrow 4_1^+)$ value is observed in the $N = 90$ isotones of Nd, Sm, and Gd. Similar to the result of ^{162}Yb, the experimental $B(E2;\ 8_1^+ \rightarrow 6_1^+)$ value is in good agreement with the X(5) prediction. These comparisons are possible because of the reduction in uncertainty in the lifetimes obtained in the present work.

Since the X(5) model is a parameter-free prediction utilizing an approximate nuclear potential, it is not surprising that perfect agreement with the experimental data is not obtained. Improved agreement should be possible with a more flexible theoretical model. In the framework of the interacting boson approximation model, fits to the Yb and Hf isotopic chains were performed in Ref. [32] using the extended consistent Q Hamiltonian [33] involving two free parameters. From the parameters obtained in those fits, the predictions of the IBA for the yrast $B(E2)$ values in ^{162}Yb and ^{166}Hf are given in Table I. The IBA calculations are also included in Fig. 8. Despite two additional parameters, the agreement for yrast $B(E2)$ values does not improve, with the IBA generally underpredicting the values. However, the contrast between these two models is interesting. In both nuclei, X(5) fails for the $6_1^+ \rightarrow 4_1^+$ transitions, where the aforementioned dip occurs, and is in good agreement with the data for the $8_1^+ \rightarrow 6_1^+$ transitions. In contrast, the IBA reproduces the $B(E2;\ 6_1^+ \rightarrow 4_1^+)$ values well but fails for the $8_1^+ \rightarrow 6_1^+$ transitions.

Note that the reason for the difference between X(5) and the IBA in this regard stems from a fundamental difference in the philosophy of the two models. In X(5), the yrast $B(E2)$ values increase monotonically, approaching a constant value, similar to the geometric rotor. In the IBA, the finite boson number results in a parabolic behavior of these $B(E2)$ values with spin. For these nuclei, the $B(E2)$ values maximize at about $J = 10^+$ or 12^+ and already show significant finite number effects ($\sim$50% reductions) at spin 8^+. The discrepancy for the IBA at higher spins measured here may reflect the difficulties with its applicability in this spin regime where finite particle number effects occur or may have other origins (e.g., other intrinsic degrees of freedom absent from the IBA). This is an important ancillary topic of considerable interest that could be investigated with a systematic study of yrast band lifetimes in deformed nuclei with plunger techniques.

From the above comparisons, it appears that the low-lying states of ^{162}Yb and ^{166}Hf are well described using a collective

model with a β-soft, γ-rigid potential given by the X(5) critical point model. The parameter-free X(5) model provides a better description of the yrast band $B(E2)$ strengths in ^{166}Hf than the two-parameter IBA calculations. In ^{162}Yb, the structure is somewhat more ambiguous, with some transitions agreeing with the X(5) predictions and others supporting more the IBA predictions or the predictions of a deformed symmetric rotor. Overall, however, the comparison of the available data on ^{162}Yb and ^{166}Hf suggests that they exhibit a similar level of agreement with the X(5) predictions as has been shown for the $N = 90$ isotones of Nd-Dy. These results provide evidence that nuclei manifesting an X(5)-like structure are not constrained to $N = 90$, and a reasonable level of agreement with the X(5) predictions is seen in nuclei in this mass region with $N = 92$ and $N = 94$.

V. CONCLUSION

RDDS lifetime measurements were performed on yrast states in ^{162}Yb and ^{166}Hf. The present results were found to be consistent within error with most of the previous measurements and yielded a significant reduction in the uncertainties of yrast band level lifetimes. The derived $B(E2)$ values show good agreement with the X(5) critical point model, with the exception of the $B(E2; 6_1^+ \rightarrow 4_1^+)$ value, which lies below the X(5) predictions in both nuclei. These results suggest that the X(5) model provides a good description of nuclei with $N = 92$ (^{162}Yb) and $N = 94$ (^{166}Hf) in the rare-earth region. Two-parameter IBA calculations were found to provide a less satisfactory description of the yrast $B(E2)$ strengths above spin 6^+, possibly linked to a finite boson number effect.

ACKNOWLEDGMENTS

Valuable discussions with F. Iachello are acknowledged. We are grateful to A. Dewald for his patience and expertise in the dismantling and reconstruction of the plunger chamber and to J. R. Cooper for his assistance with the operation of the plunger. This work was supported by U.S. DOE Grant Nos. DE-FG02-91ER-40609 and DE-FG02-88ER-40417.

[1] G. Scharff-Goldhaber and J. Weneser, Phys. Rev. **98**, 212 (1955).
[2] A. Bohr, Mat. Fys. Medd. K. Dan. Vidensk. Selsk. **26**, 1 (1952).
[3] L. Wilets and M. Jean, Phys. Rev. **102**, 788 (1956).
[4] F. Iachello, Phys. Rev. Lett. **85**, 3580 (2000).
[5] F. Iachello, Phys. Rev. Lett. **87**, 052502 (2001).
[6] M. A. Caprio, Phys. Rev. C **72**, 054323 (2005).
[7] R. Krücken *et al*., Phys. Rev. Lett. **88**, 232501 (2002).
[8] R. F. Casten and N. V. Zamfir, Phys. Rev. Lett. **87**, 052503 (2001).
[9] D. Tonev, A. Dewald, T. Klug, P. Petkov, J. Jolie, A. Fitzler, O. Möller, S. Heinze, P. von Brentano, and R. F. Casten, Phys. Rev. C **69**, 034334 (2004).
[10] M. A. Caprio *et al*., Phys. Rev. C **66**, 054310 (2002).
[11] M. A. Caprio, Phys. Rev. C **69**, 044307 (2004).
[12] Dennis Bonatsos, D. Lenis, N. Minkov, P. P. Raychev, and P. A. Terziev, Phys. Rev. C **69**, 014302 (2004).
[13] N. Pietralla and O. M. Gorbachenko, Phys. Rev. C **70**, 011304(R) (2004).
[14] J.E. Garcìa-Ramos, J. M. Arias, J. Barea, A. Frank, Phys. Rev. C **68**, 024307 (2003).
[15] R. M. Clark *et al*., Phys. Rev. C **68**, 037301 (2003).
[16] P. G. Bizzeti and A. M. Bizzeti-Sona, Phys. Rev. C **66**, 031301(R) (2002).
[17] C. Hutter *et al*., Phys. Rev. C **67**, 054315 (2003).
[18] R. G. Helmer and C. W. Reich, Nucl. Data Sheets **87**, 317 (1999).
[19] E. N. Shurshikov and N. V. Timofeeva, Nucl. Data Sheets **67**, 45 (1992).
[20] E. A. McCutchan *et al*., Phys. Rev. C **69**, 024308 (2004).
[21] E. A. McCutchan, N. V. Zamfir, R. F. Casten, M. A. Caprio, H. Ai, H. Amro, C. W. Beausang, A. A. Hecht, D. A. Meyer, and J. J. Ressler, Phys. Rev. C **71**, 024309 (2005).
[22] B. Bochev, S. A. Karamian, T. Kutsarova, E. Nadjakov, and Yu. Ts. Oganessian, Nucl. Phys. **A267**, 344 (1976).
[23] F. K. McGowan, N. R. Johnson, C. Baktash, I. Y. Lee, Y. Schutz, J. C. Wells, and A. Larabee, Nucl. Phys. **A539**, 276 (1992).
[24] B. Bochev, S. Iliev, R. Kalpakchieva, S. A. Karamian, T. Kutsarova, E. Nadjakov, and Ts. Venkova, Nucl. Phys. **A282**, 159 (1977).
[25] R. Krücken, J. Res. Natl. Inst. Stand. Technol. **105**, 53 (2000).
[26] A. Dewald *et al*., Nucl. Phys. **A545**, 822 (1992).
[27] R. Krücken, in *Proceedings of the International Symposium on Advances in Nuclear Physics, Bucharest, Romania, 1999*, edited by D. Poenaru and S. Stoica (World Scientific, Singapore, 2000), p. 336.
[28] A. Dewald, S. Harissopulos, and P. von Brentano, Z. Phys. A **334**, 163 (1989).
[29] G. Böhm, A. Dewald, P. Petkov, and P. von Brentano, Nucl. Instrum. Methods Phys. Res. A **329**, 248 (1993).
[30] F. Iachello and A. Arima, *The Interacting Boson Model* (Cambridge University Press, Cambridge England, 1987).
[31] A. Dewald *et al*., Eur. Phys. J. A **20**, 173 (2003).
[32] E. A. McCutchan, N. V. Zamfir, and R. F. Casten, Phys. Rev. C **69**, 064306 (2004).
[33] P. O. Lipas, P. Toivonen, and D. D. Warner, Phys. Lett. **B155**, 295 (1985).